Article:
Marchesi, C, Garrido, CJ, Harvey, J et al. (2013) Platinum-group elements, S, Se and Cu in highly depleted abyssal peridotites from the Mid-Atlantic Ocean Ridge (ODP Hole 1274A): Influence of hydrothermal and magmatic processes. Contributions to Mineralogy and Petrology, 166 (5). 1521 - 1538. ISSN: 0010-7999

https://doi.org/10.1007/s00410-013-0942-x

Platinum-group elements, S, Se and Cu in highly depleted abyssal peridotites from the Mid-Atlantic Ocean Ridge (ODP Hole 1274A): Influence of hydrothermal and magmatic processes

Claudio Marchesi [a*], Carlos J. Garrido [a], Jason Harvey [b], José María González-Jiménez [c], Károly Hidas [a], Jean-Pierre Lorand [d], Fernando Gervilla [a, e]

a. Instituto Andaluz de Ciencias de la Tierra, CSIC-Universidad de Granada, Avenida de las Palmeras 4, 18100 Armilla (Granada), Spain. Emails: claudio@iact.ugr-csic.es; carlos.garrido@csic.es; karoly.hidas@csic.es; gervilla@ugr.es
b. School of Earth and Environment, University of Leeds, Leeds LS2 9JT, United Kingdom. Email: feejh@leeds.ac.uk
c. ARC Centre of Excellence for Core to Crust Fluid Systems (CCFS) and GEMOC National Key Centre, Department of Earth and Planetary Sciences, Macquarie University, Sydney, NSW 2109, Australia. Email: jose.gonzalez@mq.edu.au
d. Laboratoire de Planétologie et Géodynamique de Nantes, CNRS UMR 6112, Université de Nantes, 2 Rue de la Houssinère, BP 92208, 44322 Nantes Cedex 3, France. Email: jean-pierre.lorand@univ-nantes.fr
e. Departamento de Mineralogía y Petrología, Facultad de Ciencias, Universidad de Granada, Avenida Fuentenueva s/n, 18002 Granada, Spain. Email: gervilla@ugr.es

Submitted to

Contributions to Mineralogy and Petrology

[*] Address of the corresponding author: Instituto Andaluz de Ciencias de la Tierra, CSIC-Universidad de Granada, Avenida de las Palmeras 4, 18100 Armilla (Granada), Spain. Tel.: +34 958 23 00 00. Fax: +34 958 55 26 20. Email: claudio@iact.ugr-csic.es

ABSTRACT

Highly depleted harzburgites and dunites were recovered at ODP Hole 1274A, near the intersection between the Mid-Atlantic Ocean Ridge and the 15°20'N Fracture Zone. In addition to high degrees of partial melting, these peridotites underwent multiple episodes of melt-rock reaction and intense serpentinization and seawater alteration close to the seafloor. Low concentrations of Se, Cu and platinum-group elements (PGE) in harzburgites drilled at around 35-85 meters below seafloor are consistent with the consumption of mantle sulfides after high degrees (> 15-20%) of partial melting and redistribution of chalcophile and siderophile elements into PGE-rich residual microphases. Higher concentrations of Cu, Se, Ru, Rh and Pd in harzburgites from the uppermost and lowest cores testify to late reaction with a sulfide melt. Dunites formed by percolation of silica- and sulfur-undersaturated melts into enclosing low-Se harzburgites. Platinum-group and chalcophile elements were not mobilized during dunite formation and mostly preserve the signature of precursor harzburgites, except for higher Ru and lower Pt contents caused by precipitation and removal of platinum-group minerals. During serpentinization at low temperature (< 250 °C) and reducing conditions, mantle sulfides experienced desulfurization to S-poor sulfides (mainly heazlewoodite) and awaruite. Contrary to Se and Cu, sulfur does not record the magmatic evolution of peridotites but it was mostly added in hydrothermal sulfides and sulfate from seawater. Platinum-group elements were unaffected by post-magmatic low temperature processes, except Pt and Pd that may have been slightly remobilized during oxidative seawater alteration.

Keywords: abyssal peridotite; chalcophile elements; melting; melt-rock reaction; platinum-group elements; serpentinization

INTRODUCTION

Highly siderophile elements (HSE) comprise the platinum-group elements (PGE: Os, Ir, Ru, Rh, Pt, Pd), Au and Re, which have a stronger affinity for metal in planetary bodies than the chalcophile S, Se, Te and Cu (e.g., Morgan 1986; O'Neill et al. 1995; Holzheid et al. 2000). In the mantle these elements are mainly hosted within accessory sulfides (e.g., Prichard et al. 1994; Alard et al. 2000; Lorand and Alard 2001; Luguet et al. 2001) and refractory platinum-group minerals (e.g., Pearson et al. 2007; Lorand et al. 2010, 2013; Delpech et al. 2012; Fonseca et al. 2012). Magmatic processes (partial melting, crystallization, melt-rock reaction) can fractionate HSE, S, Se, Te and Cu, because during mantle melting up to moderate degrees the most refractory PGE (IPGE: Os, Ir, Ru) behave as compatible elements while the less refractory PGE (PPGE: Pt and Pd), Au, Re, S, Se, Te and Cu are more incompatible (e.g., Lorand et al. 1999; Bockrath et al. 2004; Becker et al. 2006; Brenan 2008; Helmy et al. 2010; Fischer-Gödde et al. 2011; Fellows and Canil 2012; König et al. 2012). Hence, the HSE and chalcophile elements can be used along with lithophile elements to unravel the multistage magmatic history of a mantle domain (e.g., Handler and Bennett 1999; Lorand et al. 1999, 2003, 2004, 2013; Becker et al. 2001; Büchl et al. 2002; Marchesi et al. 2010; Harvey et al. 2011). For instance, abyssal peridotites from ODP sites 895 and 920 have relatively high concentrations of Pd that have been ascribed to late Cu-Ni-Pd-rich sulfides trapped during or after melting (Rehkämper et al. 1999; Luguet et al. 2001, 2003). Moreover, geochemical studies of altered peridotites sampled as mantle xenoliths (Handler and Bennett 1999; Handler et al. 1999; Lee 2002; Lorand et al. 2003; Pearson et al. 2004) or in orogenic massifs (Lorand et al. 2000; Lorand and Alard 2010; Fischer-Gödde et al. 2011) and ocean floors (Alt and Shanks 1998, 2003; Luguet et al. 2003; Harvey et al. 2006; Liu et al. 2009) support that Os, Pd, Au, Re, S, Se and Cu may be affected by

post-magmatic hydrothermal processes at relatively low T (< 500 °C) and/or supergene weathering.

Harzburgites and dunites drilled at ODP Leg 209 site 1274, located 31 km north of the NW intersection of the Mid-Atlantic Ridge (MAR) with the 15°20'N Fracture Zone (Fig. 1), are among the most refractory abyssal peridotites recovered from mid-ocean ridges. Their lack of residual clinopyroxene, olivine Mg# (up to 0.92), spinel Cr# (up to ~ 0.5) and low contents of Al_2O_3 and heavy rare earth elements (HREE) indicate high degrees of melting (> 15-20%), possibly starting in the garnet stability field, coupled with microstructural and geochemical evidence of melt- rock reactions (Seyler et al. 2007; Godard et al. 2008). In addition, these rocks record the effects of secondary, low temperature processes, such as serpentinization and seawater-peridotite interaction (Bach et al. 2004, 2006; Paulick et al. 2006; Alt et al. 2007; Klein and Bach 2009). Site 1274 peridotites thus provide a valuable opportunity to investigate the composition of highly melt-depleted and heavily altered mantle material, and in particular to examine the behavior of peridotite-hosted PGE and chalcophile elements under a wide variety of high and low temperature conditions.

This paper discusses the processes responsible for PGE, S, Se and Cu abundances in refractory abyssal peridotites sampled from regular intervals over the 156 meters of Hole 1274A. We show that PGE-S-Se-Cu in this material record a multistage history of magmatic and hydrothermal events that caused changes from compositions expected for highly melt-depleted upper mantle.

GEOLOGICAL SETTING AND PETROGRAPHY

The 15º20'N Fracture Zone is one of the slowest spreading portions of the MAR (~ 2.5 cm/y) and has been matter of study of several geological surveys (e.g., Cannat et al. 1997; Escartín and Cannat 1999; Escartín et al. 2003; Fujiwara et al. 2003; Kelemen et

al. 2007). This spreading zone is characterized by a thinned discontinuous basaltic crust with outcrops of mantle peridotite and gabbroic intrusions on both sides of the rift valley of the spreading axis. Two concentric Bouguer negative anomalies, located at around 14º and 16ºN, coincide with magmatic centers where thick igneous crust accreted (Escartín and Cannat 1999). The region between these two gravity bull's-eyes shows relative gravity highs spatially coincident with serpentinised peridotite and gabbro representing magma-starved areas (Cannat et al. 1997). During ODP Leg 209, 19 holes were drilled at eight sites close to the 15º20'N Fracture Zone (Kelemen et al. 2007). One of these holes, Hole 1274A (3940 m below sea level), is situated on the southern margin of the 16ºN gravity low and on the western flank of the MAR axial valley (Fig. 1). This hole penetrated to a depth of 156 m below seafloor (mbsf) with 35 m of core recovery consisting of 71% harzburgite, 19% dunite, 3% gabbro and 7% fault gouge. Harzburgite dominates the upper 80 m of the hole, where rare centimeter-scale intervals of dunite were also recovered; below 80 m the amount of dunites increases. From about 95 down to 145 mbsf there are several gouge regions consisting of brecciated peridotite and gabbro and serpentine mud, interpreted as fault zones. Peridotites of Hole 1274A show variable but high degrees of serpentinization increasing from 40-80% in the upper 95 m of the hole to almost complete serpentinization (> 95%) below. Late oxidative alteration by cold seawater formed Fe-oxyhydroxide haloes along aragonite veins in the upper 90 m of the borehole (Bach et al. 2004).

For this study we selected 15 harzburgites and three dunites from Hole 1274A, previously analyzed by Harvey et al. (2006) for Re-Os isotopes. Harzburgites are coarse-grained and show relic primary silicate assemblage made up of 70-80% olivine, 15-25% orthopyroxene, < 1-5% clinopyroxene and < 2% spinel (visual modal estimations), in the range of values reported in previous works (Paulick et al. 2006;

Seyler et al. 2007; Godard et al. 2008). Minor clinopyroxene forms veins replacing orthopyroxene, fills interstitial spaces between olivine and/or orthopyroxene, or it is associated with spinel and/or base-metal sulfides (BMS) in symplectites. These textures have been interpreted as secondary in origin and produced by reaction with or crystallization of percolating melts in ultra-depleted refractory harzburgites (Harvey et al. 2006; Seyler et al. 2007; Godard et al. 2008). Dunite was interpreted as the product of orthopyroxene dissolution in highly depleted harzburgite (Harvey et al. 2006; Godard et al. 2008).

Typical alteration products are serpentine after olivine and orthopyroxene, brucite and magnetite after olivine, and rare talc and tremolite after orthopyroxene and clinopyroxene (Bach et al. 2004, 2006). Cr-spinel is virtually unaltered but some grains exhibit variably thick (< 15 μm) rims of ferrian chromite. Pseudomorphic mesh textures with relicts of primary olivine in mesh cores and serpentine/brucite-rich mesh rims are common throughout the upper cores of Hole 1274A; in many cases magnetite forms networks within serpentine and fills fractures in former olivine grains but it is never in contact with fresh olivine. Complete serpentinization of peridotites results in the replacement of fresh olivine centers by serpentine-brucite assemblages and the formation of strings and veins of magnetite (Bach et al. 2006). Non-pseudomorphic ribbon textures, consisting of a well-developed network of serrate chrysotile veins, usually coexist with pseudomorphic textures. Thin sections in which olivine is completely serpentinised occasionally preserve unaltered clinopyroxene, indicating T < 250 ºC for fluid-rock interaction (Bach et al. 2004, 2006).

ANALYTICAL METHODS

Because of their very small size, the identification and characterization of fine-grained intergrowths of BMS could only be achieved by electron microscopy techniques. Base-

metal sulfide species were characterized using their characteristic EDS spectra and micro-photographed by an Environmental Scanning Electron Microscope (ESEM) at the CIC of the University of Granada (Spain). Quantitative analyses of single BMS grains were obtained using a CAMECA SX50 instrument at the Serveis Cientificotècnics of the University of Barcelona (Spain); accelerating voltage was 25 kV, sample current 20 nA and beam diameter 2 µm. Representative results of electron microprobe analyses are listed in Table 1.

Concentrations of S, Se, Te, PGE (Ir, Ru, Rh, Pt and Pd), Au and Cu in whole-rocks were determined at the Geoscience Laboratories (Geo Labs, Sudbury, Canada). Total sulfur was analyzed by combustion of 0.5 g rock powder, sulfur oxidation to SO_2 in an oxygen rich environment and infrared adsorption; the detection limit was 100 ppm. Selenium and tellurium were analyzed by hydride generation and inductively coupled plasma mass spectrometry (ICP-MS). The samples were digested in hot concentrated acids (perchloric, 12M hydrochloric, hydrofluoric and 16M nitric) at 120 °C for one day and taken to incipient dryness at 70 °C. Large (10 g) powder aliquots permitted detection limits of 3.5 ppb and 1 ppb for Se and Te, respectively; procedural blanks were below the analytical detection limits. Precision (< 9%) and accuracy (< 5%) for this procedure at Geo Labs have been evaluated by Lorand et al. (2008) and Lorand and Alard (2010) through analyses of international peridotite standards (UB-N and JP-1) (Table 2). Iridium, Ru, Rh, Pt, Pd and Au were measured in 15 g of sample (< 100 µm mesh) by NiS fire-assay (NiS-FA) with $SnCl_2 \cdot 2H_2O$-Te co-precipitation and ICP-MS following the procedure described by Richardson and Burnham (2002) and Savard et al. (2010). Noble metals were collected in a nickel sulfide bead, then dissolved in HCl, co-precipitated with Te, re-dissolved in aqua regia and diluted prior to ICP-MS analysis by a Perkin-Elmer ELAN 5000 device, using cadmium and thallium as drift

monitors and a PGE-Au stock solution for external calibration. Concentrations of HSE were determined from ^{193}Ir, ^{101}Ru, ^{103}Rh, ^{195}Pt, ^{105}Pd and ^{197}Au, and the data of Cu, Ni and Ta were used to monitor isobaric interferences on Ru, Rh, Pd and Au; two procedural blanks were below the detection limits. The choice of the NiS-FA technique allowed the analysis of representative large test portion mass (15 g), reducing the nugget effect that is particularly important in serpentinised peridotites, and permitted to determine mono-isotopic Rh and Au. Savard et al. (2010) have shown that the NiS-FA procedure yields analytical results comparable to data obtained by Isotope Dilution in combination with High-Pressure Asher digestion for the analyses of low-level PGE concentrations in ultramafic rocks (Table 2). Detection limits in this study were 0.03 ppb for Ir, 0.09 ppb for Ru, 0.03 ppb for Rh, 0.10 ppb for Pt, 0.06 ppb for Pd and 0.27 ppb for Au. A duplicate PGE-Au analysis of a 15 gram aliquot of sample 03R-1-61-71 is reported in Table 2; the reproducibility for all the elements in better than 3%. PGE-Au analyses of three aliquots of the CANMET Certified Reference Material TDB-1 and two aliquots of the GSJ standard JP-1, having PGE concentrations similar to the unknowns, compare well with published values of these materials (Table 2; Shirai et al. 2003; Meisel and Moser 2004; Savard et al. 2010).

Copper was determined by aqua regia digestion followed by ICP-MS analysis calibrated with external standards. 1 g of sample was attacked for one day using combination of concentrated hydrochloric and nitric acids; the detection limit was 0.7 ppm. Concentrations of chalcophile elements and PGE are displayed in Table 2. Although the data for S, Se-Te, PGE-Au and Cu were obtained from different powder aliquots, the large sample sizes processed minimize the potential effects of powder heterogeneity on the results.

RESULTS

Base-metal sulfide (BMS) mineralogy

We inspected five thin sections per sample to search for BMS and platinum-group minerals in the studied Hole 1274A peridotites. Despite careful optical observation, platinum-group minerals were not detected and BMS have only been observed in six polished sections from the upper 80 m of the borehole. The scarcity of BMS in these samples (< 0.01 vol.%) contrasts with their higher abundance detected by Seyler et al. (2007), who report up to 0.1 vol.% of BMS in samples with high modal clinopyroxene/orthopyroxene from the uppermost and lowest cores. Such a discrepancy is most likely due to the highly heterogeneous distribution of BMS between different hand samples and thin sections.

Only ~ 10% of about 180 counted grains of BMS are enclosed in fresh olivine or pyroxene and were protected from the strong serpentinization that affected the peridotites. Thus, most of the BMS occur in zones of alteration such as the contacts between olivine or pyroxene and serpentine (~ 40%) or in the serpentine matrix (~ 50%). The size of BMS grains is very variable ranging from < 1 up to > 200 µm, with a diameter of < 10 µm being typical. Base-metal sulfides hosted in fresh olivine and pyroxene have only been observed in harzburgite 02R-1-31-37 and they consist of (< 50 µm) intergrowths of pentlandite ± chalcopyrite ± bornite (Cu_5FeS_4) exhibiting bleb-like, holly leaf or more commonly subhedral shapes (Fig. 2a-c). Where hosted in pyroxene, the BMS grains are oriented parallel to the cleavage planes and are often surrounded by tails of several smaller (< 5 µm) BMS inclusions veining the host pyroxene (Fig. 2a). The occurrence of these BMS assemblages as inclusions in primary silicates and the coexistence in the BMS aggregates of Ni-rich pentlandite [Ni/Fe_{at} = 1.08-1.61, $metal/S_{at}$ = 1.02-1.13, Co < 3.57 at%] and Cu-rich sulfides (chalcopyrite, bornite) suggest their

derivation from droplets of immiscible Cu-enriched Ni-Fe sulfide melts segregated at high temperature, as proposed by Seyler et al. (2007).

Base-metal sulfides located at the contact between olivine or pyroxene and serpentine consist of ovoid/rounded droplets or irregular shaped grains of pentlandite rimmed by intergrowths of awaruite (Ni_3Fe) ± magnetite (Fig. 2d-f) (see also Klein and Bach 2009). The morphology and composition of pentlandite [Ni/Fe_{at} = 0.97-1.14, $metal/S_{at}$ = 1.03-1.06, Co < 0.87 at%] support its magmatic origin. Some grains rimmed by awaruite ± magnetite are Fe- and S-depleted [Ni/Fe_{at} = 4.85-5.48, $metal/S_{at}$ = 1.30-1.37, Co < 2.39 at%], evidencing that formation of awaruite ± magnetite occurred via desulfurization of the pre-existing pentlandite. Euhedral to subhedral grains of desulfurized cobaltian pentlandite [Ni/Fe_{at} = 1.61, $metal/S_{at}$ = 1.31, Co = 16.02 at%] replaced by heazlewoodite (Ni_3S_2) or jaipurite (CoS) coexist with Co-free pentlandite in some thin sections (Fig. 2g), in agreement with the relatively low temperature of serpentinization of these rocks (Klein and Bach 2009). Assemblages of BMS found exclusively embedded in serpentine also include pentlandite replaced by awaruite ± magnetite (Fig. 2h-i), cobaltian pentlandite replaced by heazlewoodite, jaipurite or awaruite (Fig. 2j), as well as intergrowths of pentlandite and awaruite both mantled by magnetite (Fig. 2k); in the latter case, textures suggest that awaruite co-precipitated in equilibrium with pentlandite rather than to be its low-temperature product of desulfurization (Klein and Bach 2009). Locally, pseudomorphs of pentlandite together with anhedral jaipurite, euhedral alloys (awaruite, wairauite (CoFe)) and native copper occur in the serpentine matrix (Fig. 2l-n).

Whole-rock S, Se and Cu

Hole 1274A peridotites are generally richer in sulfur (< 100-2200 ppm) than the primitive upper mantle (PUM = 250 ppm, McDonough and Sun 1995) and the depleted

mantle source of MORB (DMM = 119 ppm, Salters and Stracke 2004) (Fig. 3). Sulfur in these rocks is more abundant at a given Se than in common continental and oceanic peridotites, and its highest concentrations resemble those of some MAR abyssal peridotites (Luguet et al. 2003) (Fig. 3). The abundances of Se are more homogeneous and generally lower than in other oceanic peridotites, the PUM and DMM (Fig. 3), in agreement with the particularly depleted nature of these abyssal mantle rocks. Selenium is especially poor (< 3-8 ppb) in harzburgites and dunites from the intermediate cores (~ 35-85 mbsf) and it is richer (11-33 ppb) in harzburgites above and below this level. Selenium and S do not correlate and S/Se (~ 10^4-10^5) in all the samples is notably higher than in CI chondrite (Palme and Jones 2003), the PUM and DMM (Fig. 3). Tellurium is mostly below the analytical detection limit (1 ppb) except in three high-Se harzburgites (Te = 3-10 ppb) with Se/Te between 3 and 5, similar to values in highly refractory melting residues (Lorand and Alard 2010). Copper (2-18 ppm) is not correlated with S and Se (Fig. 4) and it is poorer than in the PUM, DMM and most continental and oceanic peridotites, especially in low-Se harzburgites (Fig. 4). Cu/S (< 0.01-0.09) is significantly lower than in the PUM (Fig. 4a), suggesting secondary S enrichment (Lorand and Alard 2010), and Cu/Se (~ 100-2000) varies largely above and below the values of PUM and DMM (Fig. 4b).

Platinum-group elements (PGE)

The PGE concentrations in Hole 1274A peridotites are variable and generally lower than in the DMM but overlap those of both oceanic and continental mantle rocks (Fig. 5). High-Se harzburgites from the uppermost and deepest cores have a relatively narrow range of IPGE (e.g., Ir = 1.59-3.44 ppb) and much more heterogeneous PPGE concentrations (e.g., Pd = 0.43-6.71 ppb), which are reflected by their very variable Pd_N/Ir_N ratios (0.13-2.81) (Fig. 5a). Rhodium in these rocks is slightly enriched

relatively to Ru and Pt. Low-Se harzburgites from the intermediate cores have more homogeneous PGE contents (e.g., Ir = 1.41-2.75, Pd = 0.17-2.63 ppb) and display flat to negatively sloping CI chondrite-normalized patterns (Pd_N/Ir_N = 0.07-0.83) (Fig. 5b); two of these samples are especially depleted in Pt and/or Pd (Fig. 5b). Except for the particular Pd enrichment (8.48 ppb) in one sample likely containing Pd- and Os-rich microphases (Harvey et al. 2006), dunites from the intermediate cores have negatively sloping PGE patterns and concentrations (Ir = 1.84-3.55, Pd =0.44-1.06 ppb, Pd_N/Ir_N = 0.21-0.26) analogous to low-Se harzburgites from similar depths, and their PGE patterns resemble those of replacive dunites from the Balmuccia peridotite massif (Fig. 5c) (Wang et al. 2013).

DISCUSSION

Low temperature hydrothermal alteration

As sulfides in mantle rocks are very prone to multiple post-magmatic modifications, interpretations of the PGE-S-Se-Cu variations in Hole 1274A peridotites require first an assessment of the potential effects of low T hydrothermal alteration. Serpentinization of Hole 1274A peridotites occurred at low T (< 250 °C), high pH (7-10), low water/rock ratio, and very low fO_2 ($\log fO_2 < -40$) and fS_2 ($-3 < \log fS_2 < -2$) conditions, mainly producing serpentine, brucite and magnetite after olivine and venting of H_2, H_2S and CH_4 in water columns above peridotites (Bach et al. 2004; Alt et al. 2007; Klein and Bach 2009). At these conditions primary Fe-Ni-Cu sulfides are altered to low S assemblages, as shown by the common desulfurization of pentlandite and chalcopyrite to awaruite, heazlewoodite and alloys in the thin sections studied here (Fig. 2d-m) (Alt and Shanks 1998; Seyler et al. 2007; Klein and Bach 2009). However, total S in peridotites from Hole 1274A is generally higher than in the PUM and DMM (Fig. 3) indicating that S in these rocks was mostly gained and not lost during their post-melting evolution. Indeed, most sulfur in these peridotites is present as sulfate derived from

seawater (Alt et al. 2007), although a sulfate phase was not optically detected in the studied thin sections likely owing to its presumable very low modal content (Alt and Shanks 2003). Relatively low ^{34}S contents in sulfide and sulfate are due to reduction upon cooling by microbial populations sustained by H_2 and CH_4 vents, which increased sulfide-S by deposition of hydrothermal sulfides associated with serpentine veins (Alt et al. 2007). Circulation of oxidizing, more siliceous fluids at higher T related to pyroxene serpentinization may in part explain the highest S contents at 130-145 mbsf in correspondence of frequent fault zones (Bach et al. 2006; Alt et al. 2007; Klein and Bach 2009). In summary, sulfur in Hole 1274A peridotites does not generally reflect their magmatic evolution but it is mostly controlled by low T hydrothermal processes similar to those experienced by abyssal peridotites at Hess Deep (Alt and Shanks 1998).

Selenium and copper in residual peridotites are less mobile than S during serpentinization, low temperature alteration and contamination by crustal fluids (Xiao et al. 1998; Handler et al. 1999; Lorand et al. 2003; Lorand and Alard 2010; König et al. 2012). Contrary to S, the low Se and Cu contents in Hole 1274A peridotites (Fig. 4b) are more consistent with the highly depleted nature of these rocks and the common incompatible behavior of these elements during mantle melting, and can be considered good proxies of abundances of magmatic BMS (Luguet et al. 2003). Indeed, hydrothermal sulfides in abyssal peridotites are poor in Se and have high S/Se (Yamamoto 1976; Luguet et al. 2004), supporting that their precipitation at Hole 1274A strongly increased S/Se (Fig. 3) without deeply affecting the Se budget. Higher Se and Cu abundances in high-Se harzburgites from the uppermost and lowermost cores (Fig. 4b) are in agreement with their higher modal abundances of magmatic BMS (Seyler et al. 2007), but the large variability of Cu/Se even in samples with concentrations well above their detection limits (Fig. 4b) suggests that magmatic Cu and/or Se abundances

were disturbed by hydrothermal processes, most likely by deposition of native copper during serpentinization (Seyler et al. 2007).

The mobility of PGE in aqueous fluids mainly depends on temperature, pH, oxygen and sulfur fugacities, and chlorine concentrations (Wood 1987; Fleet and Wu 1993; Xiong and Wood 2000; Maier 2005; Bell et al. 2009). Considering the T, pH, fO_2, and fS_2 conditions of serpentinization at Hole 1274A, Pt and Pd at this site may have been affected by low T remobilization as bisulfide complexes (Mountain and Wood 1988; Wood et al. 1992, 1994; Gammons and Bloom 1993; Pan and Wood 1994; Barnes and Liu 2012). However, the experimental studies of Gammons and Bloom (1993) and Pan and Wood (1994) suggest that the solubility of PPGE under conditions similar to those experienced during serpentinization at Hole 1274A would have been very low (maximum tens of ppt), thus several orders of magnitude lower than their concentrations in peridotites (from about 200 ppt up to 8 ppb). Scarce pyrite and valleriite ($4(Fe,Cu)S \cdot 3(Mg,Al)(OH)_2$) in late serpentine veinlets indicate higher fO_2 and fS_2 conditions during late seafloor alteration (Alt et al. 2007), which could have caused higher Pt and Pd mobilization into fluids (Gammons and Bloom 1993). However, the absolute values of oxygen and sulfur fugacities recorded by the stable mineral assemblage decrease with temperature and are expected to be notably low at < 150 °C (Alt and Shanks 1998; Delacour et al. 2008), thus strongly reducing the capacity of fluids to dissolve PPGE-bearing minerals during late circulation. In summary, although we cannot exclude that Pt and Pd may have been remobilized at low T, the impact of serpentinization and seafloor alteration on the magmatic PGE budgets of Hole 1274A peridotites can be considered minimal even for the samples most depleted in PPGE.

Partial melting and melt-rock reaction

The low clinopyroxene modal abundances and the fertility indices of Hole 1274A peridotites (e.g., Al_2O_3 < 0.92 wt.% on anhydrous basis) are benchmarks of high degrees of partial melting (> 15-20%) likely predating the melt-rock reactions undergone by these rocks (Seyler et al. 2007; Godard et al. 2008). Figure 6 shows the Al_2O_3 versus Se, -Cu and -PGE variations predicted by melting models in which the abundances of chalcophile elements and PGE are controlled by sulfides and different sulfide melt/silicate melt partition coefficients (D). Considering the uncertainties on the HSE composition of the fertile mantle source (i.e., the PUM or DMM) and on the sulfide-silicate partitioning during melt extraction, the concentrations of Se, Cu and PGE in low-Se harzburgites are well consistent with the values expected for highly depleted melting residues. Base-metal sulfides are completely exhausted from the residual solid after ~ 12-20% partial melting of a fertile source by pressure-dependent solubility of S in the melt (e.g., Handler and Bennett 1999; Lorand et al. 1999; Mavrogenes and O'Neill 1999; Luguet et al. 2003). This supports that the main hosts for PGE and Se in ultra-depleted peridotites, such as low-Se harzburgites from Hole 1274A, are scarce BMS and highly refractory PGE-rich microphases such as Os-Ir-Ru alloys, Pt-Ir-Os alloys and minerals of the laurite (RuS_2)-erlichmanite (OsS_2) solution series (Luguet et al. 2007; Lorand et al. 2010; Fonseca et al. 2012). Despite repeated SEM investigations, no such PGE-rich discrete microphases have been observed in the studied thin sections, probably owing to the extreme rareness and very small size of these minerals (Luguet et al. 2007). However, the generally good correlation between Ir and PPGE, which have different geochemical behaviors during mantle melting, in low-Se harzburgites (Fig. 7a, b) suggests partitioning of all their PGE into the same discrete phases of comparable refractoriness, likely platinum-group minerals and metal alloys formed at high T (Luguet et al. 2003).

Bearing in mind the uncertainties inherent to melting models, some high-Se harzburgites appear too rich in Cu and Se to be simple residues of high melting degrees (Fig. 6a, b), supporting that precipitation of Cu-Ni-rich sulfides (Fig. 2b) by melt-rock reaction increased the concentrations of these elements after melting. The general higher Ru-Rh-Pd abundances in these rocks compared to low-Se harzburgites (Fig. 6d, e, g) suggest that the concentrations of these elements were similarly enhanced by melt-rock reaction, in agreement with the high Ru-Rh-Pd composition of Cu-Ni-rich metasomatic sulfides in peridotites (Luguet et al. 2001, 2004; Lorand et al. 2008). Late precipitation of magmatic sulfides in high-Se harzburgites agrees with: 1) the lack of correlation between Ir and Pt-Pd in these rocks (Fig. 7a, b), which suggests their prevalent residence in different phases (i.e., refractory platinum-group minerals and metasomatic base-metal sulfides, respectively), and the suprachondritic Pt_N/Ir_N and Pd_N/Ir_N of some of these samples (Fig. 5a); 2) the contents of Au and Te, two strongly melt-loving chalcophile elements, which are above their detection limits in some of these rocks (Table 2) contrary to predictions of melting models (Fischer-Gödde et al. 2011; König et al. 2012); 3) the relatively high proportions of Cu-rich BMS in high-Se harzburgites (Fig. 2a-c, 0-50% Cp and Bn according to visual estimates), as customarily observed in metasomatized peridotites (Lorand and Alard 2001; Luguet et al. 2001, 2003, 2004; Lorand et al. 2004); and 4) the relatively BMS-rich character of harzburgites from the uppermost and lowest cores (Seyler et al. 2007), from which high-Se harzburgites were mostly recovered. However, the lack of correlation between Al_2O_3 and Se,-Cu,-Ru,-Rh and -Pd in high-Se harzburgites (Fig. 6) suggests that the concentrations of the latter elements mostly record reaction with a percolating sulfide melt separated from the silicate magma that precipitated secondary clinopyroxene and spinel (Seyler et al. 2007).

In spite of the higher affinity of Pt and Pd for sulfide melt than for monosulfide solid solution, the sulfide phase stable in the mantle at melting conditions (Bockrath et al. 2004), the precipitation of metasomatic sulfides in high-Se harzburgites has not particularly enriched these rocks in Pt (Fig. 6f), as reported for abyssal peridotites from the Kane Fracture Zone (KFZ) in the Atlantic Ocean (Rehkämper et al. 1999; Luguet et al. 2003). Indeed, Pt and Pd in high-Se harzburgites are correlated at lower slope than in low-Se harzburgites (Fig. 7c), possibly reflecting the partial retention of Pt in the source of the metasomatic sulfide melt. This may be due to the presence in the melting assemblage of Pt-Ir-Os alloys, which are stable at high temperature and low oxygen and sulfur fugacities in the convecting mantle (Lorand et al. 2008, 2010) and may partially decouple Pt from Pd (Peregoedova et al. 2004). However, the magmatic covariance of Pt and Pd in Hole 1274A peridotites may have been slightly disturbed by interaction with volatile-rich fluids at temperature close to the solidus (Godard et al. 2008), which can remobilize PPGE as chloride complexes (Wood 1987; Fleet and Wu 1993; Bell et al. 2009). Moreover, although the yields of Pt and Pd are close to 100% for the reference materials analyzed with the samples (Table 2), we cannot exclude that the low concentrations of Pt and Pd in some samples (Fig. 5) may partly reflect the incomplete collection of PPGE-rich micronuggets by the NiS fire-assay technique (Lorand et al. 2008).

Percolation of S-undersaturated melts in dunite channels

Dunites at Hole 1274A formed by dissolution of orthopyroxene in surrounding harzburgites induced by reaction with silica-undersaturated melts generated at greater depths (Godard et al. 2008). Dunites with a similar replacive origin in ophiolites generally have PPGE-rich patterns and radiogenic Os isotope compositions more similar to oceanic basaltic melts than to residual peridotites, as their HSE budgets are

mostly controlled by sulfides precipitated from S-saturated melts at high melt/rock ratio (e.g., Büchl et al. 2002, 2004; Hanghøj et al. 2010). Dunites at Hole 1274A have abundances of PGE and chalcophile elements generally similar to enclosing low-Se harzburgites, including their depletion in Se and PPGE typical of highly refractory melting residues (Fig. 6). This indicates that melt-rock reaction in dunites did not delete the PGE and chalcophile signatures of precursor harzburgites, as confirmed by their similar subchondritic Os isotope compositions (Harvey et al. 2006). The low abundance of sulfides in dunites and their resemblance to low-Se harzburgites in terms of chalcophile composition support the idea that the silicate melts that formed the dunite channels were S-undersaturated (Shi et al. 2007). Silicate melts ascending to shallow depths in the mantle can be S-undersaturated as the solubility of sulfur in mafic magmas increases with decreasing pressure (Mavrogenes and O'Neill 1999). Platinum-group and chalcophile elements in Hole 1274A dunites are thus likely controlled by mixing between residual platinum-group minerals and scarce BMS from precursor harzburgites, as proposed for dunites with similar PGE compositions from the Balmuccia peridotite massif (Wang et al. 2013). However, dunites at Hole 1274A mostly have higher Ru and lower Pt abundances than enclosing low-Se harzburgites (Fig. 6d, f), and these variations are not associated with clear changes in Se, Cu and Pd (Fig. 6a, b, g). This suggests that the mobilization of Ru and Pt is not related to BMS but may be due to precipitation/removal of platinum-group minerals. Relative Ru enrichment in dunites may have resulted from crystallization of Ru-rich discrete microphases (e.g., laurite, Os-Ir-Ru alloys) from S-undersaturated melts (Brenan and Andrews 2001) and possibly collected by Cr-rich spinel (Finnigan et al. 2008) upon cooling of the magmatic percolation system. On the other hand, the relative depletion in Pt suggests that Pt-rich refractory microphases (e.g., Pt-Ir-Os alloys) may have been dissolved or physically

stripped in the silicate melt that flowed through the dunite band (Lorand et al. 2004, 2010).

CONCLUSIONS

The sulfide assemblage of highly-depleted peridotites from ODP Hole 1274A shows the strong imprint of serpentinization at reducing conditions, which caused desulfurization of primary pentlandite and chalcopyrite to low-S sulfides and metal alloys. However, sulfur was mostly added and not removed during serpentinization and late seafloor alteration via precipitation of hydrothermal sulfides and seawater sulfate. Contrary to sulfur, selenium and copper mostly record the magmatic evolution of Hole 1274A peridotites prior to serpentinization. Harzburgites and dunites recovered from cores at intermediate depths have low Se and Cu concentrations, consistent with their highly depleted lithophile compositions; on the other hand, harzburgites from the uppermost and lowest cores are richer in Se and Cu (Fig. 4b) in agreement with the higher abundances of magmatic sulfides in these samples. In spite of the strong alteration of Hole 1274A peridotites, their interaction with fluids during serpentinization and seafloor alteration had a negligible impact on the PGE budgets, except for a possible slight mobilization of Pt and Pd at late oxidized conditions.

Low contents of Se, Cu and PGE in low-Se harzburgites from the intermediate cores are consistent with the high degrees of melting (> 15-20%) experienced by these rocks. Intense melting consumed primary mantle sulfides and redistributed PGE and chalcophile elements mainly into refractory platinum-group minerals such as Os-Ir-Ru and Pt-Ir-Os alloys, and minerals of the laurite-erlichmanite series. High-Se harzburgites drilled in the uppermost and lowest cores are richer in Se and Cu than expected from melting models, supporting that reaction with a sulfide melt crystallized late Cu-Ni-rich sulfides also enriched in Ru, Rh and Pd but not in Pt.

Percolation of SiO_2-S-undersaturated melts in peridotites recovered from the intermediate cores generated dunites by dissolution of orthopyroxene, while mostly conserving the PGE and chalcophile signatures of precursor low-Se harzburgites. Melt-rock reaction may have also induced the crystallization/stripping of residual PGE-rich microphases, causing the relative enrichment of dunites in Ru and their depletion in Pt.

ACKNOWLEDGMENTS

We are grateful to D. van Acken and two anonymous referees for their constructive reviews of the submitted version of the manuscript. This research used samples provided by the Ocean Drilling Program (ODP). ODP is sponsored by the U.S. National Science Foundation and participating countries under the management of the Joint Oceanographic Institutions (JOI) Inc. C.M.'s research has been supported by a JAE-DOC postdoctoral fellowship of the CSIC co-funded by the European Social Fund, and by a Marie Curie European Re-integration Grant under contract agreement PERG08-GA-2010-276867. This is contribution XXX from the ARC Centre of Excellence for Core to Crust Fluid Systems (http://www.ccfs.mq.edu.au) and XXX from the GEMOC Key Centre (http://www.gemoc.mq.edu.au).

REFERENCES

Alard O, Griffin WL, Lorand J-P, Jackson SE, O'Reilly SY (2000) Non-chondritic distribution of the highly siderophile elements in mantle sulphides. Nature 407:891-894

Alard O, Lorand J-P, Reisberg L, Bodinier J-L, Dautria J-M, O'Reilly SY (2011) Volatile-rich metasomatism in Montferrier xenoliths (southern France): Implications for the abundances of chalcophile and highly siderophile elements in the subcontinental mantle. J Petrol 52:2009-2045

Aldanmaz E, Meisel T, Celik OF, Henjes-Kunst F (2012) Osmium isotope systematics and highly siderophile element fractionation in spinel-peridotites from the Tethyan ophiolites in SW Turkey: Implications for multi-stage evolution of oceanic upper mantle. Chem Geol 294-295:152-164

Alt JC, Shanks III WC (1998) Sulfur in serpentinized oceanic peridotites: Serpentinization processes and microbial sulfate reduction. J Geophys Res 103(B5):9917-9929

Alt JC, Shanks III WC (2003) Serpentinization of abyssal peridotites from the MARK area, Mid-Atlantic Ridge: Sulfur geochemistry and reaction modeling. Geochim Cosmochim Acta 67:641-653

Alt JC, Shanks III WC, Bach W, Paulick H, Garrido CJ, Beaudoin G (2007) Hydrothermal alteration and microbial sulfate reduction in peridotite and gabbro exposed by detachment faulting at the Mid-Atlantic Ridge, 15°20'N (ODP Leg 209): A sulfur and oxygen isotope study. Geochem Geophys Geosyst 8(8):Q08002

Bach W, Garrido CJ, Paulick H, Harvey J, Rosner M (2004) Seawater-peridotite interactions: First insights from ODP Leg 209, MAR 15°N. Geochem Geophys Geosyst 5(9):Q09F26

Bach W, Paulick H, Garrido CJ, Ildefonse B, Meurer WP, Humphris SE (2006) Unraveling the sequence of serpentinization reactions: petrography, mineral chemistry, and petrophysics of serpentinites from MAR 15°N (ODP Leg 209, Site 1274). Geophys Res Lett 33:L13306

Barnes S-J, Savard D, Bédard LP, Maier WD (2009) Selenium and sulfur concentrations in the Bushveld Complex of South Africa and implications for formation of the platinum-group element deposits. Miner Deposita 44:647-663

Barnes SJ, Liu W (2012) Pt and Pd mobility in hydrothermal fluids: Evidence from komatiites and from thermodynamic modelling. Ore Geol Rev 44:49-58

Becker H, Shirey SB, Carlson RW (2001) Effects of melt percolation on the Re-Os systematics of peridotites from a Paleozoic convergent plate margin. Earth Planet Sci Lett 188:107-121

Becker H, Horan MF, Walker RJ, Gao S, Lorand J-P, Rudnick RL (2006) Highly siderophile element composition of the Earth's primitive upper mantle: Constraints from new data on peridotite massifs and xenoliths. Geochim Cosmochim Acta 70:4528-4550

Bell AS, Simon A, Guillong M (2009) Experimental constraints on Pt, Pd and Au partitioning and fractionation in silicate melt-sulfide-oxide-aqueous fluid systems at 800 °C, 150 MPa and variable sulfur fugacity. Geochim Cosmochim Acta 73:5778-5792

Bockrath C, Ballhaus C, Holzheid A (2004) Fractionation of the platinum-group elements during mantle melting. Science 305:1951-1953

Brenan JM (2008) Re-Os fractionation by sulfide melt-silicate melt partitioning: A new spin. Chem Geol 248:140-165

Brenan JM, Andrews D (2001) High-temperature stability of laurite and Ru-Os-Ir alloy and their role in the PGE fractionation in mafic magmas. Can Mineral 39:341-360

Büchl A, Brügmann G, Batanova VG, Münker C, Hofmann AW (2002) Melt percolation monitored by Os isotopes and HSE abundances: a case study from the mantle section of the Troodos Ophiolite. Earth Planet Sci Lett 204:385-402

Büchl A, Brügmann G, Batanova VG, Hofmann AW (2004) Os mobilization during melt percolation: The evolution of Os isotope heterogeneities in the mantle sequence of the Troodos ophiolite, Cyprus. Geochim Cosmochim Acta 68:3397-3408

Cannat M, Lagabrielle Y, de Coutures N, Bougault H, Casey J, Dmitriev L, Fouquet Y (1997) Ultramafic and gabbroic exposures at the Mid-Atlantic Ridge: Geological mapping in the 15ºN region. Tectonophys 279:193-213

Crocket JH, Fleet ME, Stone WE (1997) Implications of composition for experimental partitioning of platinum-group elements and gold between sulfide liquid and basalt melt: The significance of nickel content. Geochim Cosmochim Acta 61:4139-4149

Delacour A, Früh-Green GL, Bernasconi SM, Kelley DS (2008) Sulfur in peridotites and gabbros at Lost City (30°N, MAR): Implications for hydrothermal alteration

and microbial activity during serpentinization. Geochim Cosmochim Acta 72:5090-5110
Delpech G, Lorand J-P, Grégoire M, Cottin J-Y, O'Reilly SY (2012) In-situ geochemistry of sulfides in highly metasomatized mantle xenoliths from Kerguelen, southern Indian Ocean. Lithos 154:296-314
Escartín J, Cannat M (1999) Ultramafic exposures and the gravity signature of the lithosphere near the Fifteen-Twenty Fracture Zone (Mid-Atlantic Ridge, 14°-16.5°N). Earth Planet Sci Lett 171:411-424
Escartín J, Mével C, MacLeod CJ, McCaig AM (2003) Constraints on deformation conditions and the origin of oceanic detachments: The Mid-Atlantic Ridge core complex at 15°45′N. Geochem Geophys Geosyst 4(8):1067
Fellows SA, Canil D (2012) Experimental study of the partitioning of Cu during partial melting of Earth's mantle. Earth Planet Sci Lett 337-338:133-143
Finnigan CS, Brenan JM, Mungall JE, McDonough WF (2008) Experiments and models bearing on the role of chromite as a collector of Platinum group minerals by local reduction. J Petrol 49:1647-1665
Fischer-Gödde M, Becker H, Wombacher F (2011) Rhodium, gold and other highly siderophile elements in orogenic peridotites and peridotite xenoliths. Chem Geol 280:365-383
Fleet ME, Wu T-W (1993) Volatile transport of platinum-group elements in sulfide-chloride assemblages at 1000°C. Geochim Cosmochim Acta 57:3519-3531
Fleet ME, Crocket JH, Liu M, Stone WE (1999) Laboratory partitioning of platinum-group elements (PGE) and gold with application to magmatic sulfide-PGE deposits. Lithos 47:127-142
Fonseca ROC, Laurenz V, Mallmann G, Luguet A, Hoehne N, Jochum KP (2012) New constraints on the genesis and long-term stability of Os-rich alloys in the Earth's mantle. Geochim Cosmochim Acta 87:227-242
Fujiwara T, Lin J, Matsumoto T, Kelemen PB, Tucholke BE, Casey JF (2003) Crustal evolution of the Mid-Atlantic Ridge near the Fifteen-Twenty Fracture Zone in the last 5 Ma. Geochem Geophys Geosyst 4(3):1024
Gammons CH, Bloom MS (1993) Experimental investigation of the hydrothermal geochemistry of platinum and palladium: II. The solubility of PtS and PdS in aqueous sulfide solutions to 300°C. Geochim Cosmochim Acta 57:2451-2467
Godard M, Lagabrielle Y, Alard O, Harvey J (2008) Geochemistry of the highly depleted peridotites drilled at ODP Sites 1272 and 1274 (Fifteen-Twenty Fracture Zone, Mid-Atlantic Ridge): Implications for mantle dynamics beneath a slow spreading ridge. Earth Planet Sci Lett 267:410-425
Handler MR, Bennett VC (1999) Behaviour of platinum-group elements in the subcontinental mantle of eastern Australia during variable metasomatism and melt depletion. Geochim Cosmochim Acta 63:3597-3618
Handler MR, Bennett VC, Dreibus G (1999) Evidence from correlated Ir/Os and Cu/S for late-stage Os mobility in peridotite xenoliths: Implications for Re-Os systematics. Geology 27:75-78
Hanghøj K, Kelemen PB, Hassler D, Godard M (2010) Composition and genesis of depleted mantle peridotites from the Wadi Tayin massif, Oman ophiolite; major and trace element geochemistry, and Os isotope and PGE systematics. J Petrol 51:201-227
Harvey J, Gannoun A, Burton KW, Rogers NW, Alard O, Parkinson IJ (2006) Ancient melt extraction from the oceanic upper mantle revealed by Re-Os isotopes in abyssal peridotites from the Mid-Atlantic ridge. Earth Planet Sci Lett 244:606–

621
Harvey J, Dale CW, Gannoun A, Burton KW (2011) Osmium mass balance in peridotite and the effects of mantle-derived sulphides on basalt petrogenesis. Geochim Cosmochim Acta 75:5574-5596
Helmy HM, Ballhaus C, Wohlgemuth-Ueberwasser C, Fonseca ROC, Laurenz V (2010) Partitioning of Se, As, Sb, Te and Bi between monosulfide solid solution and sulfide melt - Application to magmatic sulfide deposits. Geochim Cosmochim Acta 74:6174-6179
Holzheid A, Sylvester P, O'Neill HSC, Rubie DC, Palme H (2000) Evidence for a late chondritic veneer in the Earth's mantle from high-pressure partitioning of palladium and platinum. Nature 406:396-399.
Kelemen PB, Kikawa E, Miller DJ, Party SS (2007) Leg 209 summary: Processes in a 20-km-thick conductive boundary layer beneath the Mid-Atlantic Ridge, 14°-16°N. Proc Ocean Drill Progr Sci Results 209 doi:10.2973/odp.proc.sr.2209.2001.2007
Klein F, Bach W (2009) Fe-Ni-Co-O-S phase relations in peridotite-seawater interactions. J Petrol 50:37-59
König S, Luguet A, Lorand J-P, Wombacher F, Lissner M (2012) Selenium and tellurium systematics of the Earth's mantle from high precision analyses of ultra-depleted orogenic peridotites. Geochim Cosmochim Acta 86:354-366
Lee C-TA (2002) Platinum-group element geochemistry of peridotite xenoliths from the Sierra Nevada and the Basin and Range, California. Geochim Cosmochim Acta 66:3987-4005
Liu C-Z, Snow JE, Brügmann G, Hellebrand E, Hofmann AW (2009) Non-chondritic HSE budget in Earth's upper mantle evidenced by abyssal peridotites from Gakkel ridge (Arctic Ocean). Earth Planet Sci Lett 283:122-132
Lorand J-P, Alard O (2001) Platinum-group element abundances in the upper mantle: New constraints from in situ and whole-rock analyses of Massif Central xenoliths (France). Geochim Cosmochim Acta 65:2789-2806
Lorand J-P, Alard O (2010) Determination of selenium and tellurium concentrations in Pyrenean peridotites (Ariege, France): New insight into S/Se/Te systematics of the upper in mantle samples. Chem Geol 278:120-130
Lorand J-P, Pattou L, Gros M (1999) Fractionation of platinum-group elements and gold in the upper mantle: a detailed study in Pyrenean orogenic lherzolites. J Petrol 40:957-981
Lorand J-P, Schmidt G, Palme H, Kratz K-L (2000) Highly siderophile element geochemistry of the Earth's mantle: new data for the Lanzo (Italy) and Ronda (Spain) orogenic peridotite bodies. Lithos 53:149-164
Lorand J-P, Alard O, Luguet A, Keays RR (2003) Sulfur and selenium systematics of the subcontinental lithospheric mantle: Inferences from the Massif Central xenolith suite (France). Geochim Cosmochim Acta 67:4137-4151
Lorand J-P, Delpech G, Grégoire M, Moine B, O'Reilly SY, Cottin J-Y (2004) Platinum-group elements and the multistage metasomatic history of Kerguelen lithospheric mantle (South Indian Ocean). Chem Geol 208:195-215
Lorand J-P, Luguet A, Alard O, Bezos A, Meisel T (2008) Abundance and distribution of platinum-group elements in orogenic lherzolites; a case study in a Fontete Rouge lherzolite (French Pyrénées). Chem Geol 248:174-194
Lorand J-P, Alard O, Luguet A (2010) Platinum-group element micronuggets and refertilization process in Lherz orogenic peridotite (northeastern Pyrenees, France). Earth Planet Sci Lett 289:298-310

Lorand J-P, Luguet A, Alard O (2013) Platinum-group element systematics and petrogenetic processing of the continental upper mantle: A review. Lithos 164-167:2-21

Luguet A, Alard O, Lorand J-P, Pearson NJ, Ryan C, O'Reilly SY (2001) Laser-ablation microprobe (LAM)-ICPMS unravels the highly siderophile element geochemistry of the oceanic mantle. Earth Planet Sci. Lett 189:285-294

Luguet A, Lorand J-P, Seyler M (2003) Sulfide petrology and highly siderophile element geochemistry of abyssal peridotites: A coupled study of samples from the Kane Fracture Zone (45°W 23°20N, MARK Area, Atlantic Ocean). Geochim Cosmochim Acta 67:1553-1570

Luguet A, Lorand J-P, Alard O, Cottin J-Y (2004) A multi-technique study of platinum group element systematic in some Ligurian ophiolitic peridotites, Italy. Chem Geol 208:175-194

Luguet A, Shirey SB, Lorand J-P, Horan MF, Carlson RW (2007) Residual platinum-group minerals from highly depleted harzburgites of the Lherz massif (France) and their role in HSE fractionation of the mantle. Geochim Cosmochim Acta 71:3082-3097

Maier WD (2005) Platinum-group element (PGE) deposits and occurrences: Mineralization styles, genetic concepts, and exploration criteria. J Afr Earth Sci 41:165-191

Marchesi C, Griffin WL, Garrido CJ, Bodinier J-L, O'Reilly SY, Pearson NJ (2010) Persistence of mantle lithospheric Re-Os signature during asthenospherization of the subcontinental lithospheric mantle: insights from in situ isotopic analysis of sulfides from the Ronda peridotite (Southern Spain). Contrib Mineral Petrol 159:315-330

Mavrogenes JA, O'Neill HSC (1999) The relative effects of pressure, temperature and oxygen fugacity on the solubility of sulfide in mafic magmas. Geochim Cosmochim Acta 63:1173-1180

McDonough WF, Sun S-s (1995) The composition of the Earth. Chem Geol 120:223-253

Meisel T, Moser J (2004) Reference materials for geochemical PGE analysis: new analytical data for Ru, Rh, Pd, Os, Ir, Pt and Re by isotope dilution ICP-MS in 11 geological reference materials. Chem Geol 208:319-338

Morgan JW (1986) Ultramafic xenoliths: clues to Earth's late accretionary history. J Geophys Res 91(B12):12375-12387

Mountain BW, Wood SA (1988) Chemical controls on the solubility, transport and deposition of platinum and palladium in hydrothermal solutions: A thermodynamic approach. Econ Geol 83:492-510

O'Neill HSC, Dingwell DB, Borisov A, Spettel B, Palme H (1995) Experimental petrochemistry of some highly siderophile elements at high temperatures, and some implications for core formation and the mantle's early history. Chem Geol 120:255-273

Palme H, Jones A (2003) Solar system abundances of the elements. In: Davis AM (ed) Meteorites, Comets and Planets, Treatise Geochemistry 1. Elsevier, Oxford, pp 41-61

Pan P, Wood SA (1994) Solubility of Pt and Pd sulfides and Au metal in aqueous bisulfide solutions II. Results at 200° to 350 °C and saturated vapor pressure. Miner Depos 29:373-390

Paulick H, Bach W, Godard M, De Hoog JCM, Suhr G, Harvey J (2006) Geochemistry of abyssal peridotites (Mid-Atlantic Ridge, 15°20′N, ODP Leg 209): Implications

for fluid/rock interaction in slow spreading environments. Chem Geol 234:179-210
Peach CL, Mathez EA, Keays RR (1990) Sulfide melt-silicate melt distribution coefficients for noble metals and other chalcophile elements as deduced from MORB: Implications for partial melting. Geochim Cosmochim Acta 54:3379-3389
Pearson DG, Irvine GJ, Ionov DA, Boyd FR, Dreibus GE (2004) Re-Os isotope systematics and platinum group element fractionation during mantle melt extraction: a study of massif and xenolith peridotite suites. Chem Geol 208:29-59
Pearson DG, Parman SW, Nowell GM (2007) A link between large mantle melting events and continent growth seen in osmium isotopes. Nature 449:202-205
Peregoedova A, Barnes S-J, Baker DR (2004) The formation of Pt-Ir alloys and Cu-Pd-rich sulfide melts by partial desulfurization of Fe-Ni-Cu sulfides: results of experiments and implications for natural systems. Chem Geol 208:247-264
Prichard HM, Ixer RA, Lord RA, Maynard J, Williams N (1994) Assemblages of platinum-group minerals and sulfides in silicate lithologies and chromite-rich rocks within the Shetland ophiolite. Can Mineral 32:271-294
Rehkämper M, Halliday AN, Alt J, Fitton JG, Zipfel J, Takazawa E (1999) Non-chondritic platinum-group element ratios in oceanic mantle lithosphere: petrogenetic signature of melt percolation? Earth Planet Sci Lett 172:65-81
Richardson T, Burnham OM (2002) Precious metal analysis at the Geoscience Laboratories: results from the new low-level analytical facility. Ontario Geol Surv Open File Rep 6100:35
Rose-Weston L, Brenan JM, Fei Y, Secco RA, Frost DJ (2009) Effect of pressure, temperature, and oxygen fugacity on the metal-silicate partitioning of Te, Se, and S: Implications for earth differentiation. Geochim Cosmochim Acta 73:4598-4615
Salters VJM, Stracke A (2004) Composition of the depleted mantle. Geochem Geophys Geosyst 5(5):Q05004
Savard D, Barnes S-J, Meisel T (2010) Comparison between Nickel-Sulfur Fire Assay Te co-precipitation and Isotope Dilution with High-Pressure Asher acid digestion for the determination of platinum-group elements, rhenium and gold. Geostand Geoanal Res 34:281-291
Seyler M, Lorand J-P, Dick HJB, Drouin M (2007) Pervasive melt percolation reactions in ultra-depleted refractory harzburgites at the Mid-Atlantic Ridge, 15° 20': ODP Hole 1274A. Contrib Mineral Petrol 153:303-319
Shi R, Alard O, Zhi X, O'Reilly SY, Pearson NJ, Griffin WL, Zhang M, Chen X (2007) Multiple events in the Neo-Tethyan oceanic upper mantle: Evidence from Ru-Os-Ir alloys in the Luobusa and Dongqiao ophiolitic podiform chromitites, Tibet. Earth Planet Sci Lett 261:33-48
Shirai N, Nishino T, Li X, Amakawa Y, Ebihara M (2003) Precise determination of PGE in a GSJ reference sample JP-1 by ID-ICPMS after nickel sulfide fire assay preconcentration. Geochem J 37:531-536
Snow JE, Schmidt G (1998) Constraints on Earth accretion deduced from noble metals in the oceanic mantle. Nature 391:166-169
Snow JE, Schmidt G, Rampone E (2000) Os isotopes and highly siderophile elements (HSE) in the Ligurian ophiolites, Italy. Earth Planet Sci Lett 175:119-132
van Acken D, Becker H, Hammerschmidt K, Walker RJ, Wombacher F (2010) Highly siderophile elements and Sr–Nd isotopes in refertilized mantle peridotites - A case study from the Totalp ultramafic body, Swiss Alps. Chem Geol 276:257-268
Wang Z, Becker H, Gawronski T (2013) Partial re-equilibration of highly siderophile

elements and the chalcogens in the mantle: A case study on the Baldissero and Balmuccia peridotite massifs (Ivrea Zone, Italian Alps). Geochim Cosmochim Acta 108:21-44

Wood SA (1987) Thermodynamic calculations of the volatility of the platinum group elements (PGE): The PGE content of fluids at magmatic temperatures. Geochim Cosmochim Acta 51:3041-3050

Wood SA, Mountain BW, Pan P (1992) The aqueous geochemistry of platinum, palladium and gold: recent experimental constraints and re-evaluation of theoretical predictions. Canad Mineral 30:955-982

Wood SA, Pan P, Zhang Y, Mucci A (1994) The solubility of Pt and Pd sulfides and Au in bisulfide solutions I. Results at 25°-90 °C and 1 bar pressure. Miner Depos 29:309-317

Xiao Z, Gammons CH, Williams-Jones AE (1998) Experimental study of copper(I) chloride complexing in hydrothermal solutions at 40 to 300°C and saturated water vapor pressure. Geochim Cosmochim Acta 62:2949-2964

Xiong Y, Wood SA (2000) Experimental quantification of hydrothermal solubility of platinum-group elements with special reference to porphyry copper environments. Mineral Petrol 68:1-28

Yamamoto M (1976) Relationship between Se/S and sulfur isotope ratios of hydrothermal sulfide minerals. Miner Deposita 11:197-209

FIGURE CAPTIONS

Fig. 1 Bathymetric map showing the geographic location of ODP Leg 209 site 1274 (star) in the Atlantic Ocean, north to the NW intersection between the axial valley of the Mid-Atlantic Ridge (MAR) and the 15°20'N Fracture Zone (FZ); modified after Paulick et al. (2006)

Fig. 2 Back-scattered electron images of sulfide, oxide and native metal assemblages in peridotites of Hole 1274A. a) Base-metal opaque minerals included in coarse orthopyroxene (Opx) partially replaced by serpentine (Srp). b) and c) Composite aggregates of pentlandite (Pn), chalcopyrite (Cp) and bornite (Bn) hosted in unaltered orthopyroxene of figure a). d), e) and f) Pentlandite partially replaced by intergrowths of awaruite (Aw) ± magnetite (Mt) at the contacts between orthopyroxene or spinel (Spl) and serpentine. g) Cobaltian pentlandite (Co-Pn) replaced along rims by jaipurite (Jp) at contact between olivine and serpentine. h) Desulfurized pentlandite rimmed by awaruite and i) awaruite + magnetite in the serpentine matrix. j) Cobaltian pentlandite replaced by awaruite in serpentine after olivine. k) Intergrowths of pentlandite and awaruite

mantled by magnetite in serpentine vein. l) Euhedral awaruite embedded in serpentine. m) Wairauite (Wa) associated with magnetite and n) native copper (Cu) in the serpentine matrix

Fig. 3 Se (ppb) versus S (ppm) concentrations in Hole 1274A peridotites. Black squares: low-Se harzburgites from cores 06R3-13R1; grey circles: dunites from cores 8R1, 8R2 and 16R1; white squares: high-Se harzburgites from cores 01R1-5R2 and 15R1-27R1. Compositions of oceanic peridotites (small black circles) are from Lorand et al. (2004) and Luguet et al. (2003), and of continental peridotites (small white circles) are from Alard et al. (2011), König et al. (2012), Lorand and Alard (2001, 2010), Lorand et al. (2003), Morgan (1986) and Wang et al. (2013). PUM (grey star) and DMM (black star) are from McDonough and Sun (1995) and Salters and Stracke (2004), respectively

Fig. 4 a) S versus Cu (ppm) and b) Se (ppb) versus Cu (ppm) in Hole 1274A peridotites. Symbols as in figure 3. Oceanic peridotites from Hanghøj et al. (2010) and Lorand et al. (2004) and continental peridotites from Alard et al. (2011), König et al. (2012), Lorand and Alard (2001, 2010) and Lorand et al. (1999, 2003). PUM (grey star) and DMM (black star) are from McDonough and Sun (1995) and Salters and Stracke (2004), respectively

Fig. 5 Chondrite-normalized PGE patterns of high-Se harzburgites (a), low-Se harzburgites (b) and dunites (c) from Hole 1274A. Normalizing values from Palme and Jones (2003). Symbols as in figure 3. PGE compositions of oceanic peridotites (grey field) in (a) and (b) are from Aldanmaz et al. (2012), Becker et al. (2006), Büchl et al. (2002), Hanghøj et al. (2010), Lorand et al. (2004), Luguet et al. (2001, 2003, 2004), Rehkämper et al. (1999), Snow and Schmidt (1998), Snow et al. (2000) and van Acken et al. (2010). PGE compositions of continental peridotites (dashed line) in (a) and (b)

are from Alard et al. (2011), Becker et al. (2006), Handler and Bennett (1999), Lee (2002), Lorand and Alard (2001), Lorand et al. (1999, 2000, 2010), Pearson et al. (2004), Rehkämper et al. (1999) and Wang et al. (2013). Field of oceanic dunites (dashed line) in (c) is from Aldanmaz et al. (2012), Büchl et al. (2002), Hanghøj et al. (2010), Lorand et al. (2004) and Rehkämper et al. (1999); PGE patterns of the Balmuccia dunites (grey lines) are from Wang et al. (2013)

Fig. 6 Comparison of Se (a), Cu (b) and PGE (c-g) compositions of Hole 1274A peridotites with predictions of batch melting models (solid lines) based on different sulfide melt-silicate melt partition coefficients (D). Al_2O_3 values (wt.% on anhydrous basis) from Harvey et al. (2006). Symbols as in figure 3. The grey star shows the PUM composition of McDonough and Sun (1995) and the white box its variability inferred by Becker et al. (2006). Melting is modelled using a primitive upper mantle source with S = 250 ppm and S solubility in melt = 1000 ppm. D values in (a) are from Barnes et al. (2009) and Rose-Weston et al. (2009), in (b) are from Barnes et al. (2009) and Fellows and Canil (2012), and in (c, d, e, f, g) are from Peach et al. (1990), Crocket et al. (1997), Fleet et al. (1999) and Handler and Bennett (1999); small black circles indicate the percentages of melt extraction. The compositions of abyssal peridotites from the Kane Fracture Zone (KFZ, Atlantic Ocean) (Rehkämper et al. 1999; Luguet et al. 2003; Becker et al. 2006) are shown for comparison (dashed area)

Fig. 7 Ir versus Pt (a) and Pd (b), and Pd versus Pt (c) in Hole 1274A peridotites. All concentrations are in ppb. Symbols as in figure 3 and melting models as in figure 6 (solid lines). The grey star shows the average composition of the PUM (Becker et al. 2006). The compositions of abyssal peridotites from the Kane Fracture Zone (KFZ, Atlantic Ocean) (Rehkämper et al. 1999; Luguet et al. 2003; Becker et al. 2006) are shown for comparison (dashed area)

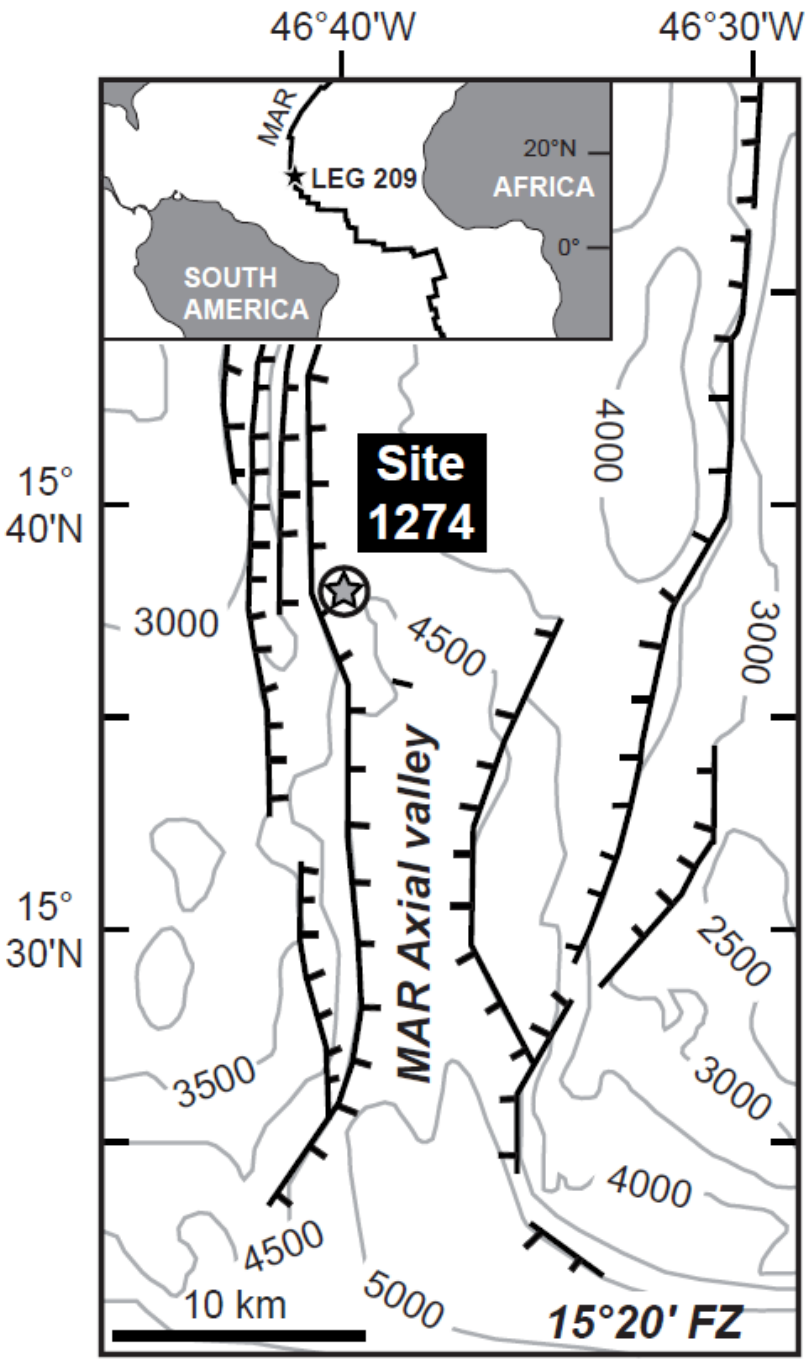
46°40'W
46°30'W
MAR
LEG 209
20°N
AFRICA
0°
SOUTH
AMERICA
Site
1274
15°
40'N
15°
30'N
4000
3000
4500
3000
MAR Axial valley
2500
3500
3000
4000
4500
10 km
5000
15°20' FZ

Figure 2
Click here to download high resolution image

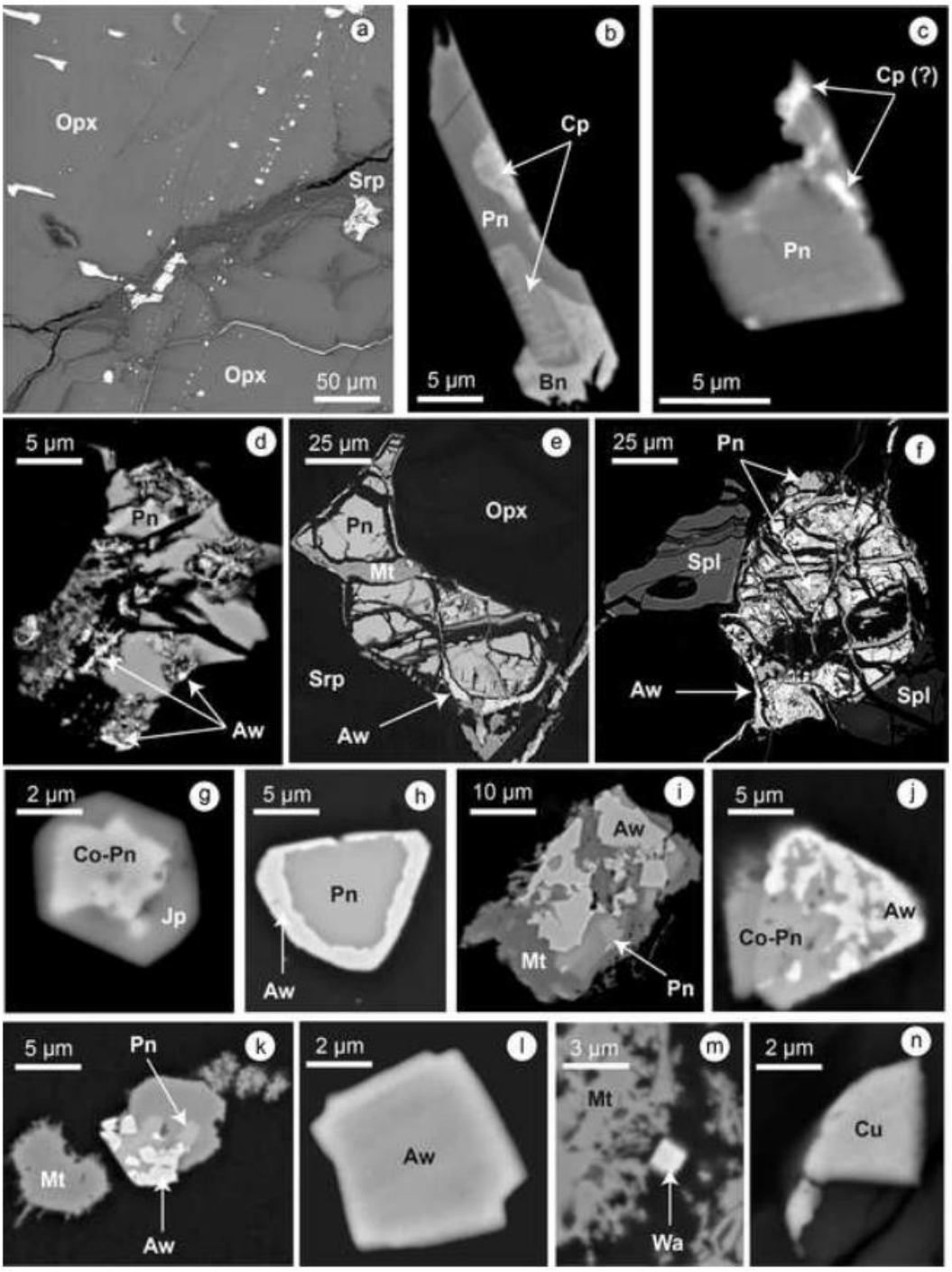

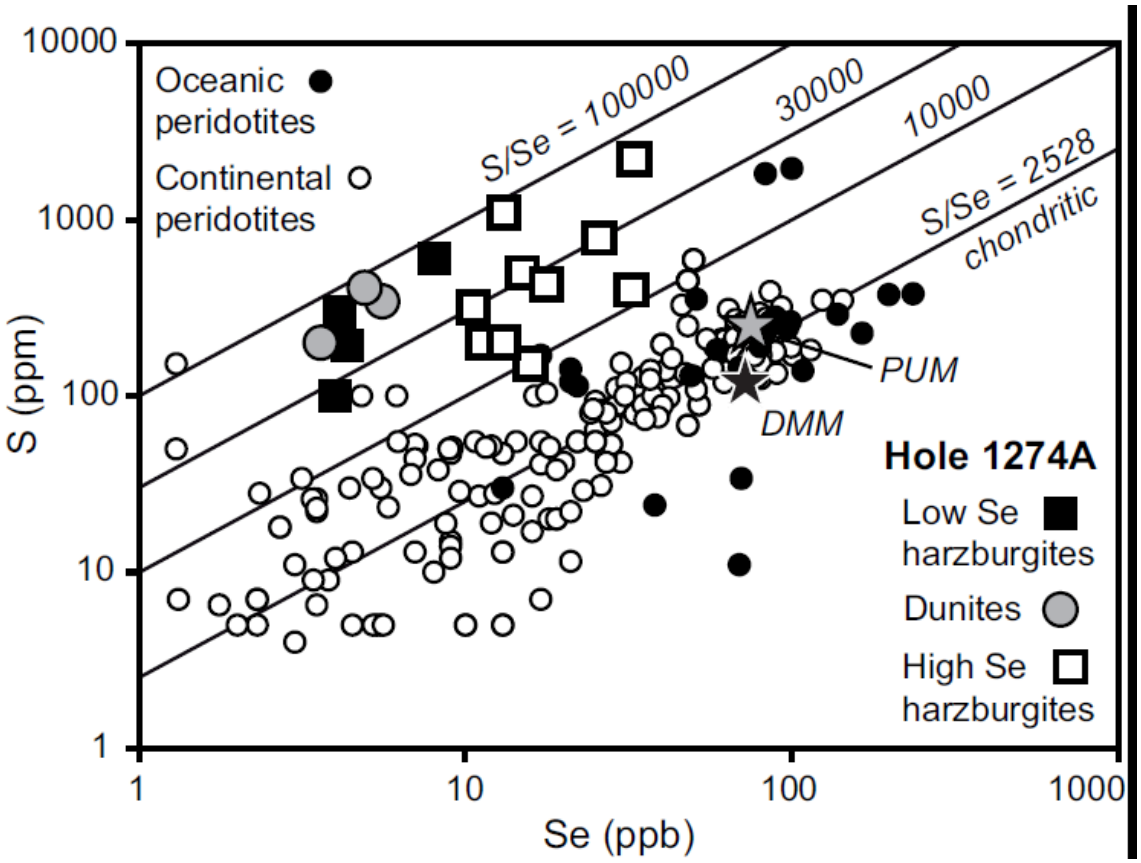
10000
1000
100
10
1
S (ppm)
1
10
100
1000
Se (ppb)
Oceanic peridotites
Continental peridotites
S/Se = 100000
30000
10000
S/Se = 2528
chondritic
PUM
DMM
Hole 1274A
Low Se harzburgites
Dunites
High Se harzburgites

Figure 4
Click here to download Figure: Figure 4.eps

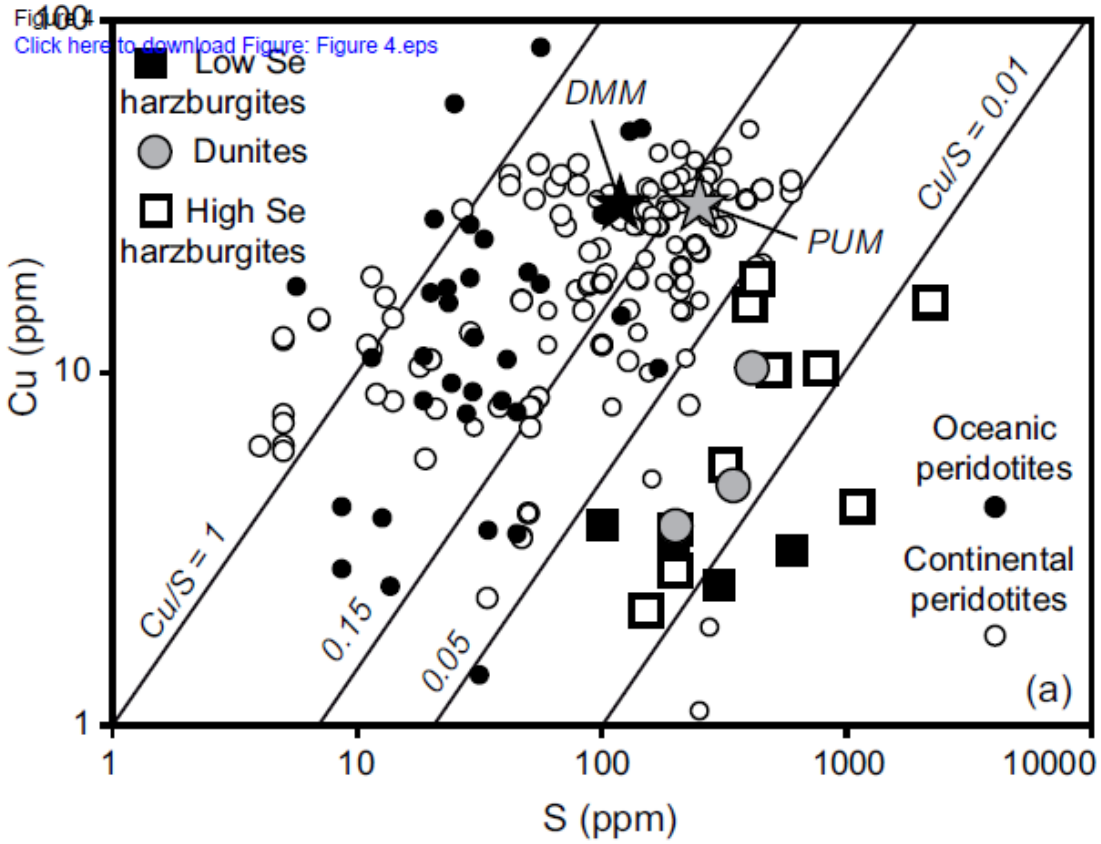

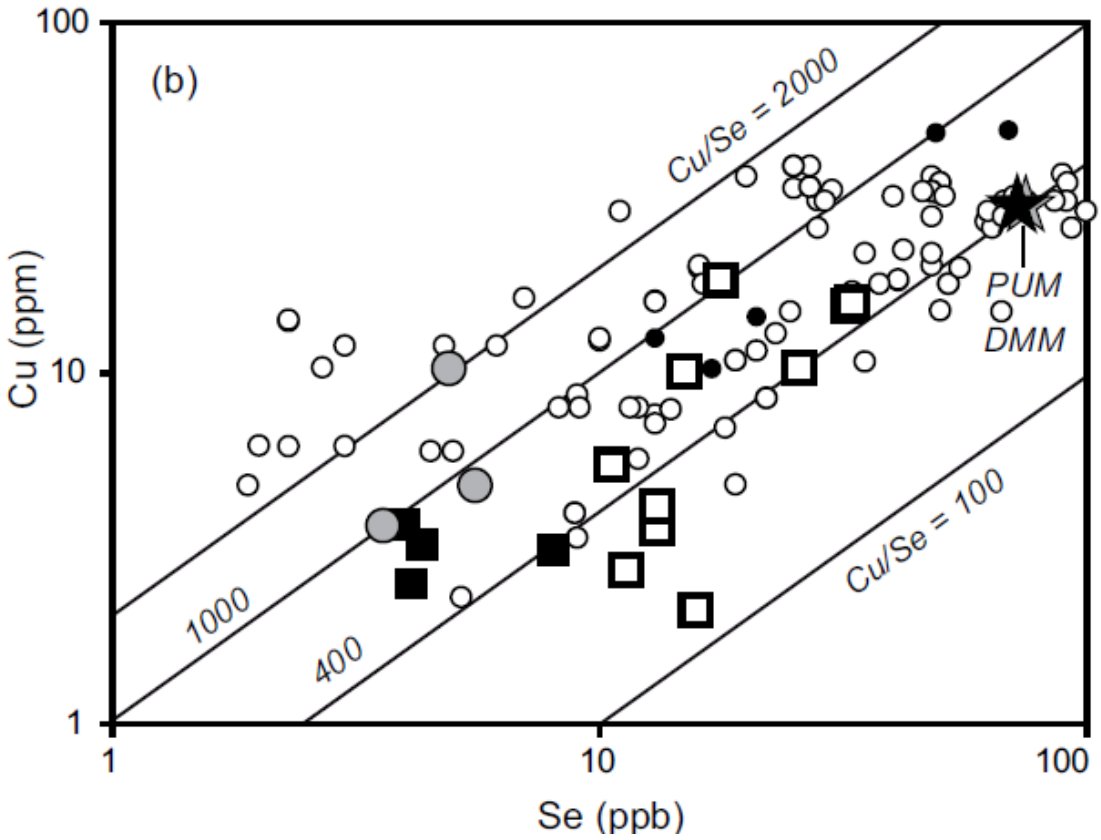

Figure 5

Click here to download Figure: Figure 5.eps

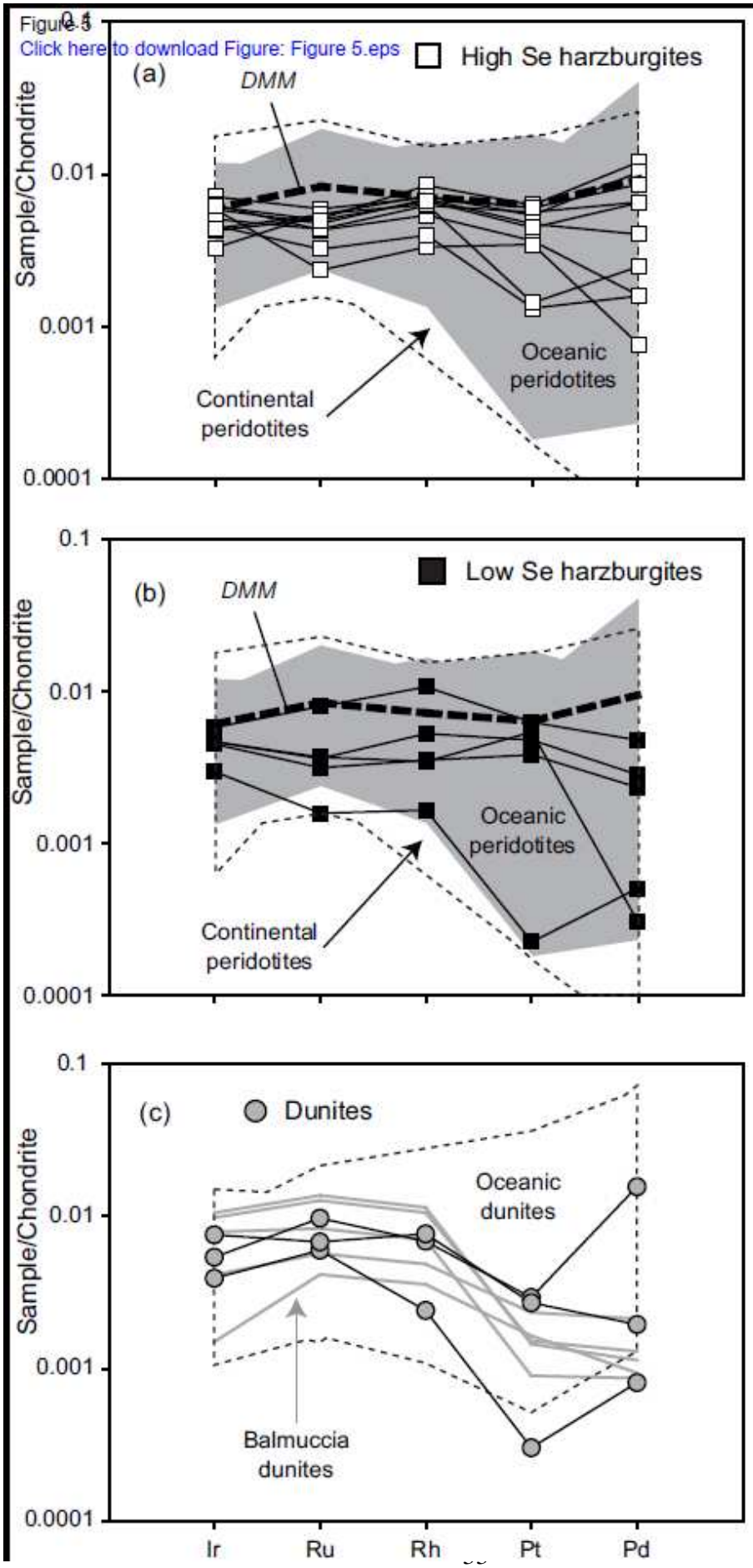

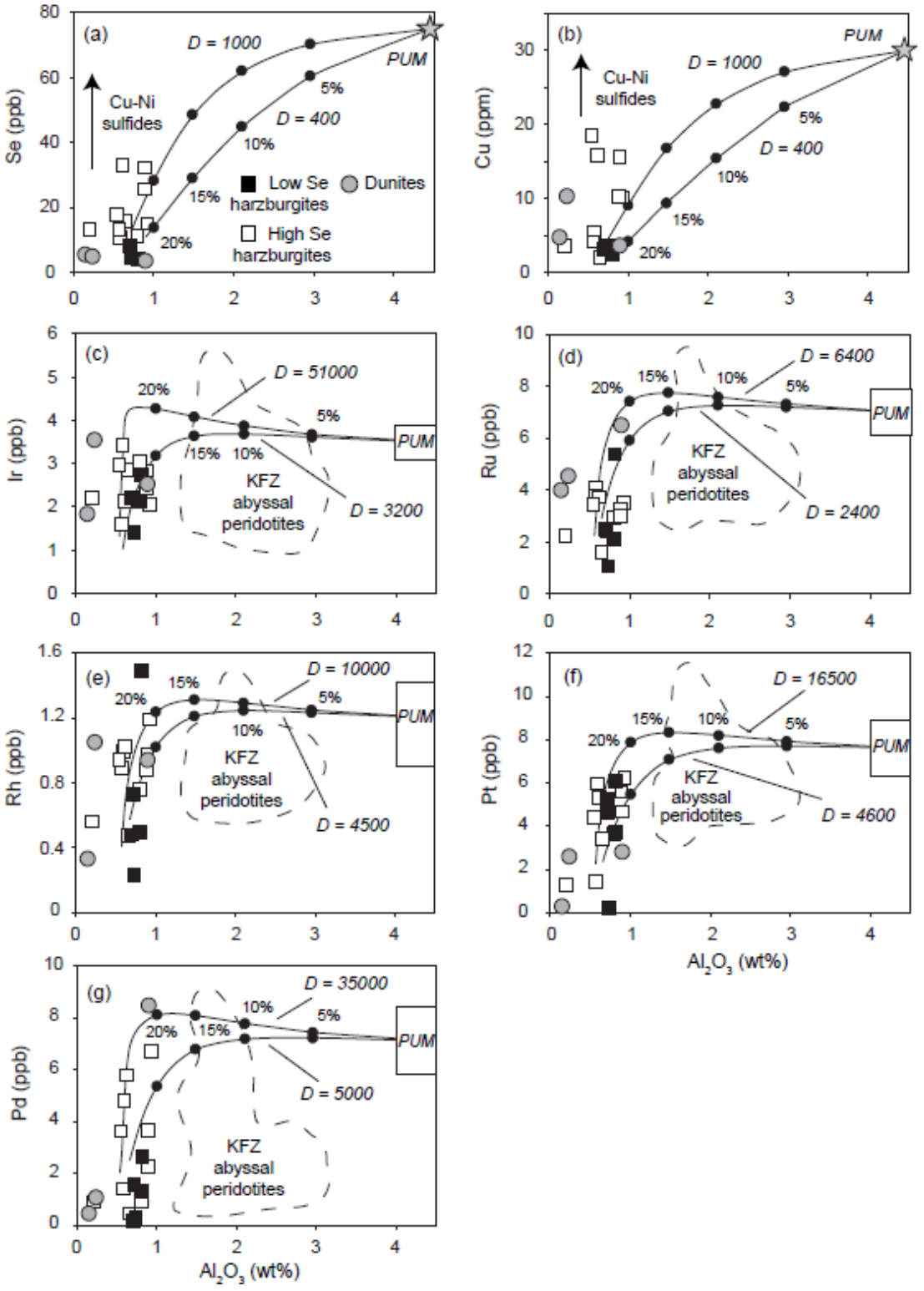
(a)
D = 1000
PUM
5%
D = 400
10%
15%
20%
Cu-Ni sulfides
Low Se harzburgites
Dunites
High Se harzburgites
Se (ppb)
(b)
PUM
D = 1000
Cu-Ni sulfides
5%
D = 400
10%
15%
20%
Cu (ppm)
(c)
D = 51000
20%
5%
PUM
15%
10%
KFZ abyssal peridotites
D = 3200
Ir (ppb)
(d)
D = 6400
20%
15%
10%
5%
PUM
KFZ abyssal peridotites
D = 2400
Ru (ppb)
(e)
D = 10000
15%
20%
5%
PUM
10%
KFZ abyssal peridotites
D = 4500
Rh (ppb)
(f)
D = 16500
15%
10%
20%
5%
PUM
KFZ abyssal peridotites
D = 4600
Pt (ppb)
(g)
D = 35000
10%
5%
20%
15%
PUM
D = 5000
KFZ abyssal peridotites
Pd (ppb)
Al2O3 (wt%)
Al2O3 (wt%)

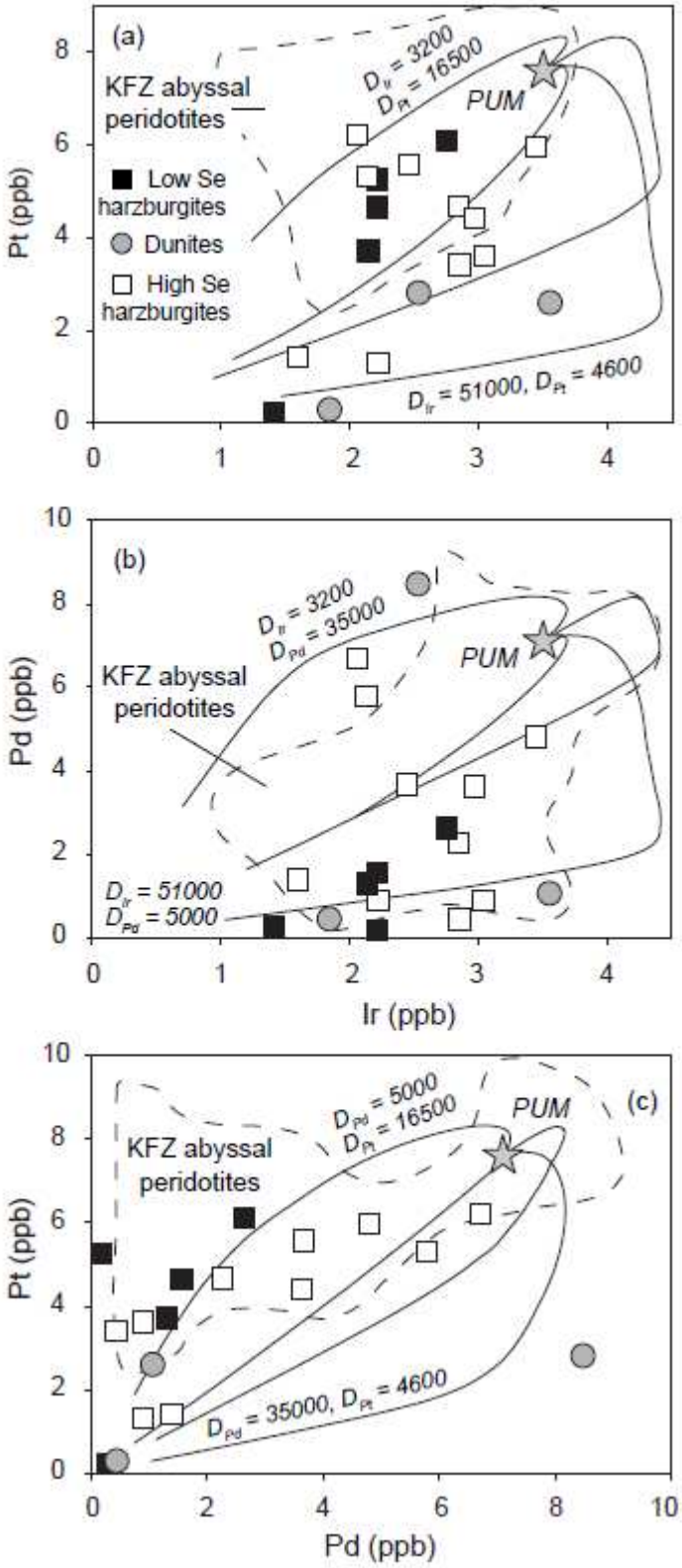
(a)
KFZ abyssal peridotites
Low Se harzburgites
Dunites
High Se harzburgites
D_{Ir} = 3200
D_{Pt} = 16500
PUM
D_{Ir} = 51000, D_{Pt} = 4600
Pt (ppb)
(b)
D_{Ir} = 3200
D_{Pd} = 35000
PUM
KFZ abyssal peridotites
D_{Ir} = 51000
D_{Pd} = 5000
Pd (ppb)
Ir (ppb)
(c)
D_{Pd} = 5000
D_{Pt} = 16500
PUM
KFZ abyssal peridotites
D_{Pd} = 35000, D_{Pt} = 4600
Pt (ppb)
Pd (ppb)

Table 1. Representative electron microprobe analyses of sulfides and their alteration products in Hole 1274A peridotites

Core-section	02R-1				02R-1						02R-1						
Interval (cm)	31-37				31-37						31-37						
Depth (mbsf)	12.27				12.27						12.27						
Lithology	High Se harzburgite				High Se harzburgite						High Se harzburgite						Hi
Microstructure	Inclusion in orthopyroxene				Contact orthopyroxene-serpentine						Contact olivine-serpentine						Emb
Mineral	Pentlandite	Pentlandite	Pentlandite	Pentlandite	Pentlandite	Pentlandite	Pentlandite	Awaruite	Awaruite	Awaruite	Desulfurized pentlandite	Desulfurized pentlandite	Desulfurized Co-pentlandite	Awaruite	Awaruite	Awaruite	Pentandite
Fe (wt%)	28.52	24.86	30.45	30.28	30.00	32.46	29.46	26.23	24.71	27.15	10.10	11.79	18.92	23.58	23.08	23.65	26.00
Ni	32.51	42.16	34.64	35.15	35.44	33.23	35.42	73.21	74.20	71.87	58.14	60.09	32.01	74.97	74.63	74.65	32.19
Co	4.79	0.97	0.92	0.78	0.77	1.09	1.17	0.06	0.10	0.11	3.05	0.41	20.56	0.50	0.55	0.42	7.96
Cu	0.04	0.13	0.19	0.20	0.06	0.10	0.15	0.27	0.65	0.57	0.16	0.24	0.07	0.83	1.47	1.13	0.10
S	33.92	31.74	33.59	33.50	33.45	33.10	33.51	0.04	0.20	0.15	28.33	27.29	28.33	0.06	0.02	0.01	33.67
Total	99.78	99.85	99.80	99.91	99.72	99.97	99.71	99.82	99.86	99.86	99.78	99.82	99.89	99.94	99.75	99.86	99.92
Fe (at%)	22.43	19.88	23.99	23.86	23.67	25.62	23.24	27.22	25.62	28.13	8.34	9.80	15.56	24.49	24.03	24.59	20.50
Ni	24.33	32.07	25.96	26.35	26.60	24.96	26.58	72.28	73.22	70.84	45.66	47.50	25.04	74.10	73.91	73.85	24.14
Co	3.57	0.73	0.69	0.59	0.57	0.81	0.87	0.06	0.10	0.11	2.39	0.32	16.02	0.49	0.54	0.42	5.95
Cu	0.03	0.09	0.13	0.14	0.04	0.07	0.11	0.25	0.59	0.52	0.11	0.17	0.05	0.76	1.34	1.03	0.07
S	49.56	47.15	49.15	49.03	49.02	48.53	49.10	0.08	0.38	0.29	43.42	42.12	43.26	0.12	0.04	0.02	49.29
Ni/Fe	1.08	1.61	1.08	1.10	1.12	0.97	1.14	2.66	2.86	2.52	5.48	4.85	1.61	3.03	3.08	3.00	1.18
Metal/S	1.02	1.12	1.03	1.04	1.04	1.06	1.03	1275	264	340	1.30	1.37	1.31	819	2449	4908	1.03

mbsf = meters below seafloor

02R-1		08R-1				01R-1			08R-1	02R-1		
31-37		72-82				40-46			72-82	31-37		
12.27		40.72				0.40			40.72	12.27		
igh Se harzburgite		Dunite				High Se harzburgite			Dunite	High Se harzburgite		
›edded in serpentine		Embedded in serpentine				Embedded in serpentine			Embedded in serpentine	Embedded in serpentine		
Pentandite	Pentandite	Desulfurized pentlandite	Desulfurized pentlandite	Co-pentlandite	Co-pentlandite	Awaruite	Awaruite	Awaruite	Awaruite	Heazlewoodite	Heazlewoodite	Heazlewoodite
30.34	27.55	27.76	28.49	7.48	5.49	23.90	23.78	24.40	22.33	11.91	8.13	5.58
31.10	33.64	45.61	39.33	12.48	12.61	75.22	75.22	73.95	76.09	64.06	60.27	66.27
7.27	5.81	4.42	5.52	45.21	50.56	0.48	0.56	1.01	0.89	0.24	4.65	1.74
0.09	0.00	0.03	0.04	0.06	0.07	0.27	0.26	0.43	0.18	0.05	0.00	0.07
31.08	32.94	22.11	26.57	34.45	31.20	0.01	0.04	0.08	0.39	23.68	26.80	26.26
99.89	99.95	99.94	99.96	99.68	99.94	99.88	99.87	99.88	99.88	99.94	99.85	99.93
24.33	21.82	23.83	23.63	5.92	4.44	24.83	24.71	25.33	23.13	10.17	6.79	4.68
23.73	25.34	37.25	31.04	9.40	9.72	74.34	74.34	73.03	74.99	52.03	47.89	52.91
5.52	4.36	3.60	4.34	33.90	38.81	0.47	0.56	0.99	0.88	0.20	3.68	1.39
0.07	0.00	0.02	0.03	0.04	0.05	0.24	0.23	0.40	0.16	0.04	0.00	0.05
46.29	48.45	35.26	40.93	50.62	46.94	0.02	0.08	0.16	0.74	37.54	41.56	40.92
0.98	1.16	1.56	1.31	1.59	2.19	2.99	3.01	2.88	3.24	5.12	7.06	11.30
1.16	1.06	1.84	1.44	0.97	1.13	5058	1261	627	134	1.66	1.40	1.44

Table 2. Whole-rock abundances of chalcophile elements and PGE in Hole 1274A peridotites

Core-section	Interval (cm)	Depth (mbsf)	Lithology	S (ppm)	Cu	Se (ppb)	Te	Ir	Ru	Rh	Pt	Pd	Au	Al_2O_3 (wt.%)	CaO
01R-1	40-46	0.40	High Se harzburgite	500	10	15	bdl	2.06	3.52	1.19	6.22	6.71	1.20	0.92	1.01
02R-1	31-37	12.27	High Se harzburgite	400	16	32	bdl	2.84	3.27	0.97	4.67	2.26	bdl	0.89	0.75
03R-1	61-71	17.51	High Se harzburgite	320	5	11	bdl	3.44	4.08	0.99	5.96	4.81	0.76	0.58	0.60
03R-1	61-71	17.51	Duplicate					3.37	4.00	0.98	5.95	4.76	0.73		
04R-1	30-36	21.60	High Se harzburgite	200	3	11	bdl	3.04	2.96	0.76	3.62	0.90	bdl	0.80	0.76
05R-2	25-35	27.99	High Se harzburgite	152	2	16	bdl	2.85	1.62	0.47	3.42	0.43	bdl	0.65	0.47
06R-3	24-34	33.06	Low Se harzburgite	bdl	4	bdl	bdl	2.21	2.45	0.73	4.66	1.56	bdl	0.71	0.95
07R-1	68-74	36.48	Low Se harzburgite	100	4	4	bdl	2.75	5.38	1.49	6.10	2.63	bdl	0.82	0.70
08R-1	72-82	40.72	Dunite	344	5	6	bdl	1.84	4.00	0.33	0.29	0.44	bdl	0.14	0.22
08R-2	1-6	41.84	Dunite	200	4	4	bdl	2.53	6.50	0.94	2.81	8.48	bdl	0.90	0.14
11R-1	56-65	55.46	Low Se harzburgite	195	3	4	bdl	1.41	1.07	0.23	0.22	0.28	bdl	0.73	0.72
12R-2	35-41	59.74	Low Se harzburgite	300	3	4	bdl	2.14	2.13	0.49	3.72	1.29	bdl	0.81	0.77
13R-1	8-14	64.84	Low Se harzburgite	600	3	8	bdl	2.21	2.50	0.48	5.26	0.17	bdl	0.70	0.33
15R-1	106-112	75.06	High Se harzburgite	200	4	13	4	2.22	2.22	0.56	1.31	0.89	bdl	0.20	0.15
16R-2	26-38	85.40	Dunite	410	10	5	bdl	3.55	4.54	1.05	2.60	1.06	bdl	0.24	0.15
24R-1	16-26	131.96	High Se harzburgite	788	10	26	bdl	2.45	3.00	0.88	5.58	3.67	0.85	0.89	0.33
25R-1	63-69	137.13	High Se harzburgite	1100	4	13	3	1.59	3.79	0.89	1.42	1.39	bdl	0.57	0.05
26R-1	76-82	142.26	High Se harzburgite	2200	16	33	10	2.13	3.73	1.02	5.31	5.79	0.92	0.61	0.17
27R-1	130-140	147.40	High Se harzburgite	430	18	18	bdl	2.97	3.44	0.94	4.42	3.63	0.78	0.55	0.42
UB-N	Lorand and Alard (2010)		Reference material			113-123	8.4-8.9								
UB-N	König et al. (2012)		Reference material			123-128	9.65-9.67								
UB-N	Wang et al. (2013)		Reference material			127	10.6								
TDB-1	n = 3		Reference material	266				0.07-0.09	0.23	0.39-0.41	4.43-4.78	21.5-22.6	5.88-6.51		
TDB-1	Meisel and Moser (2004)		Reference material					0.075	0.198	0.471	5.01	24.3			
TDB-1	Savard et al. (2010)		Reference material					0.084	0.253	0.466	4.64	22.82	4.00		
JP-1	n = 2		Reference material				1.4-1.7	3.31-3.37	6.10-6.24	0.97-1.04	3.91-4.50	1.40-1.47	bdl		
JP-1	Shirai et al. (2003)		Reference material					3.31	6.18	0.875	3.99	1.33			
JP-1	Meisel and Moser (2004)		Reference material					2.47	5.29	0.94	5.09	1.63			
JP-1	Lorand and Alard (2010)		Reference material			7.4-7.5	1.0-1.2								

mbsf = meters below seafloor; bdl = below detection limit; Al_2O_3 and CaO on anhydrous basis from Harvey et al. (2006)